Bifunctional Janus Silica Spheres for Pickering Interfacial Tandem Catalysis

Fuqiang Chang[+],[a] Carolien M. Vis[+],[b] Menno Bergmeijer,[c] Stuart C. Howes,[c] and Pieter C. A. Bruijnincx*[a]

Nature provides much inspiration for the design of multistep conversion processes, with numerous reactions running simultaneously and without interference in cells, for example. A key challenge in mimicking nature's strategies is to compartmentalize incompatible reagents and catalysts, for example, for tandem catalysis. Here, we present a new strategy for antagonistic catalyst compartmentalization. The synthesis of bifunctional Janus catalyst particles carrying acid and base groups on the particle's opposite patches is reported as is their application as acid-base catalysts in oil/water emulsions. The synthesis strategy involved the use of monodisperse, hydrophobic and amine-functionalized silica particles (SiO_2–NH_2–OSi$(CH_3)_3$) to prepare an oil-in-water Pickering emulsion (PE) with molten paraffin wax. After solidification, the exposed patch of the silica particles was selectively etched and refunctionalized with acid groups to yield acid-base Janus particles (Janus A–B). These materials were successfully applied in biphasic Pickering interfacial catalysis for the tandem dehydration-Knoevenagel condensation of fructose to 5-(hydroxymethyl)furfural-2-diethylmalonate (5-HMF-DEM) in a water/4-propylguaiacol PE. The results demonstrate the advantage of rapid extraction of 5-hydroxymethylfurfural (5-HMF), a prominent platform molecule prone to side product formation in acidic media. A simple strategy to tune the acid/base balance using PE with both Janus A–B and monofunctional SiO_2–NH_2–OSi$(CH_3)_3$ base catalysts proved effective for antagonistic tandem catalysis.

Introduction

Tandem catalysis, that is operating multiple, mechanistically distinct consecutive reactions in a 'one-pot' manner, is a highly attractive strategy to make catalytic processes more efficient.[1] This approach can eliminate costly separation steps and allows for overall process simplification, thereby increasing time, energy and resource efficiency.[2] When (multifunctional) solid catalysts are used for such tandem reactions, catalytically active structures that have no obvious incompatibility issues can simply be immobilized on a (functional) support material, for example by common deposition or chemical grafting methods. Typical examples include immobilization of noble-metal nanoparticles on zeolites[3] or graphitic carbon nitride.[4,5] However, for catalysts that are chemically incompatible, such as acid and base catalysts, spatial separation of the catalysts is necessary. Previous examples of spatially separating catalysts for heterogeneous tandem catalysis include stacked-shell materials such as core-shell, yolk-shell or multishelled hollow structures.[6–15] These materials have mainly been used for tandem reactions in one-phase reaction media. Biphasic tandem catalysis with antagonistic (e.g., acid-base) bifunctional catalysts still remains largely unexplored, however.

Biphasic oil/water systems have been extensively investigated and have demonstrated their great use in numerous organic transformations, in separation and purification.[16] Despite their extensive application, a general drawback of these systems is the low reaction efficiency due to the limited liquid/liquid interfacial area. A very efficient way to increase interfacial area, and hence reaction and/or extraction efficiency, is to place a solid at the liquid/liquid interface and create an emulsion. Recently, such solid particle-stabilized emulsions, so-called Pickering emulsions (PEs) have been receiving increased attention for their application in biphasic catalysis.[17–19] The solid particles at the boundary layer in PEs serve to compartmentalize and to protect the dispersed phase from the continuous phase, for example, allowing multiple reactions to be mediated consecutively.[20–22] The catalysts can then be dissolved in both phases, or the solid emulsifier itself can be

[a] Dr. F. Chang,[+] Prof. P. C. A. Bruijnincx
Organic Chemistry and Catalysis
Debye Institute for Nanomaterials Science
Utrecht University
Universiteitsweg 99
3584 CG Utrecht (The Netherlands)
E-mail: p.c.a.bruijnincx@uu.nl
[b] Dr. C. M. Vis[+]
Inorganic Chemistry and Catalysis
Debye Institute for Nanomaterials Science
Utrecht University
Universiteitsweg 99
3584 CG Utrecht (The Netherlands)
[c] M. Bergmeijer, Dr. S. C. Howes
Structural Biochemistry
Bijvoet Centre for Biomolecular Research
Utrecht University
Universiteitsweg 99
3584 CG Utrecht (The Netherlands)
[+] These authors contributed equally to this work.

Supporting information for this article is available on the WWW under https://doi.org/10.1002/cssc.202101238

This publication is part of a Special Collection highlighting "The Latest Research from our Board Members". Please visit the Special Collection at chemsuschem.org/collections.

endowed with catalytic properties. For the latter, the solids should then be bifunctional when acid-base catalysis is targeted. Janus particles consisting of two patches with distinct properties are particularly interesting materials in this respect. Although bifunctional Janus particles are increasingly being investigated as stabilizers for PEs, the opportunities they offer yet remain largely unexploited for PE tandem catalysis.[23,24]

Recent studies strongly suggest that the geometry as well as the surface properties of Janus particles have a significant influence on their surface activity.[25,26] To date, Janus particles shaped as spheres,[27,28] dumbbells,[29] polygons[30] or nanosheets[31,32] have been reported for the successful stabilization of PEs. Janus spheres are ideal for designing interface-active solid catalysts, as the equilibrium orientation of the Janus boundary tends to get pinned at the interface when the nonpolar and polar hemispheres are exposed to the oil and water phases, respectively.[33–35] By placing catalytically active groups on the polar and/or the nonpolar hemispheres, the interfacial configuration of the Janus spheres can be precisely controlled, and thereby, the catalytic activity in a biphasic reaction system.[36–38] The available examples of Janus sphere use in PE catalysis are mostly limited, however, to mono-catalytic materials bearing metal nanoparticle functionalities. The Janus nature of the particles is exploited to improve stability and single patch decoration allows the amount of metal nanoparticles required to be reduced.[29,37,39] Synthesizing Janus particles with antagonistic catalyst patches and opposite wettability on different patches of the Janus spheres is still a major challenge and no examples of this are, to the best of our knowledge, currently available.

Biomass valorization efforts could benefit from antagonistic tandem catalysis strategies to convert renewable biomass to high-value products. 5-Hydroxymethylfurfural (5-HMF), a key sugar-derived renewable platform molecule, is attracting much attention for the production of various biobased chemicals.[40] Significant effort has been devoted to the development of efficient methods for 5-HMF production and its conversion to value-added fine chemicals.[41–43] For example, the catalytic hydrogenation and oxidation of 5-HMF have been widely investigated[40] and 5-HMF derived furans have been used in fine chemistry.[44–47] Integrated tandem catalytic conversion of renewable sugars to value-added products via 5-HMF as intermediate nevertheless remains a significant challenge.[48–50]

Here, we present a strategy for the synthesis of bifunctional Janus PE emulsifiers to specifically locate acid and base functionalities into the two distinct liquid phases of the emulsion. The approach involved immobilizing hydrophobized amine-functionalized silica particles in a wax-based PE allowed the exposed patch of the silica particles to be selectively etched and further modified to also bear complementary acid functionalities. The acid-base functionalized Janus silica spheres were able to stabilize w/o PEs and used as solid catalytic emulsifiers for the tandem catalytic dehydration-Knoevenagel condensation of fructose (Scheme 1). The transport of 5-HMF across the interface minimizes side reactions, such as organic acid and humins formation.[51]

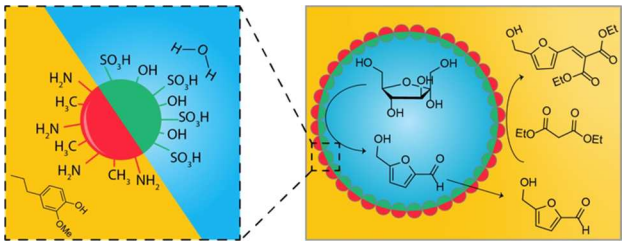

Scheme 1. Schematic representation of the use of bifunctional Janus A–B spheres for tandem PE catalysis. Left: Janus A–B particlesget pinned at the oil/water interface, spatially localizing the two catalyst functionalities in the polar (acid) and nonpolar (base) phases. Right: The dehydration-Knoevenagel condensation reaction of fructose. Blue: water droplet; yellow: continuous organic phase.

Results and Discussion

Synthesis of Janus silica with sulfonic acid and amine functional groups (Janus A–B)

A schematic representation of the general synthesis strategy is given in Scheme 2. Bifunctional Janus silica spheres with asymmetric wettability were synthesized through a solidified wax Pickering emulsion method. The wax can serve as dispersed oil phase when the temperature is above its melting point, immobilizing the silica particles at the surface of the wax droplets.[52,53] Solidification at lower temperature then fixes the configuration of the silica particles, allowing the unprotected hemisphere exposed to the aqueous phase to be modified by chemical etching or grafting, for example, by silane chemistry.

Figure 1a shows that the bare silica spheres synthesized using the Stöber method were highly uniform with an average

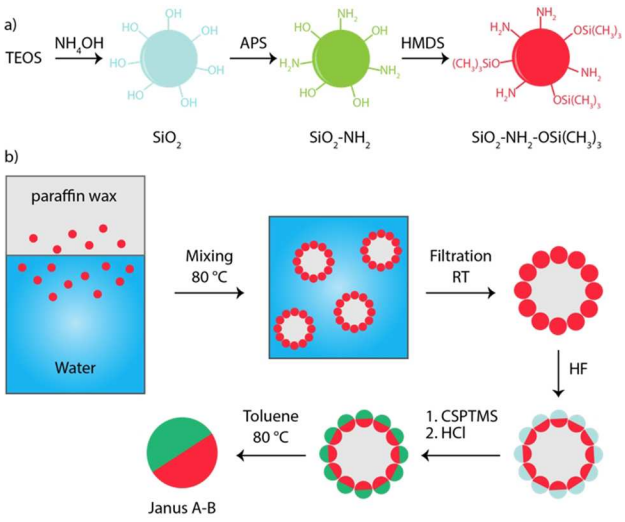

Scheme 2. a) Schematic representation of the synthesis of the monofunctional base-loaded and, hydrophobic particles synthesized from Stöber silica (SiO_2). APS = (3-aminopropyl)triethoxysilane; HMDS = hexamethyldisilazane. b) Schematic representation of the synthesis of acid-base functionalized Janus particles using the solidified wax procedure. HF = hydrofluoric acid; CSPTMS = 2-(4-chlorosulfonylphenyl)ethyltrimethoxysilane.

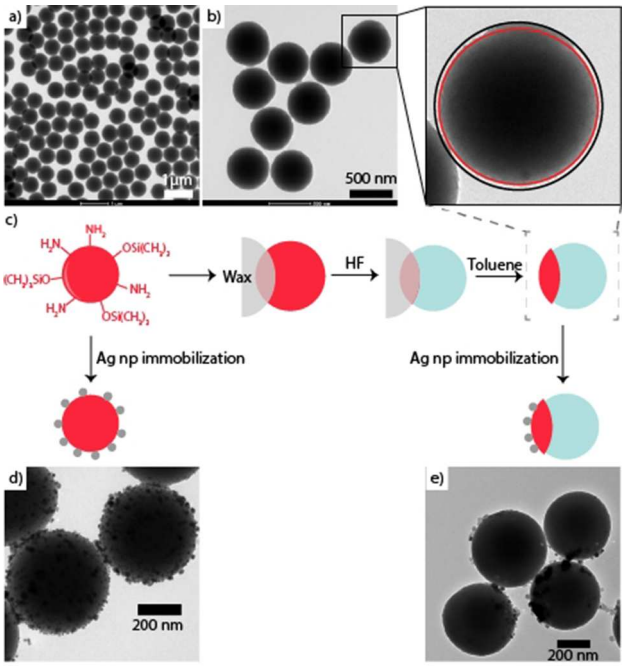

Figure 1. a, b) TEM images of SiO_2 particles synthesized via the Stöber method, (a; scale bar = 1 µm) and partially etched SiO_2–NH_2–$OSi(CH_3)_3$ particles (b; scale bar = 500 nm). Zoom shows the etched area of the particles; the black circle corresponds to the original diameter of the particle; the red circle highlights the diameter of the etched part of the particle. c) Schematic representation of etching procedure of SiO_2–NH_2–$OSi(CH_3)_3$ by solidified wax method. d, e) TEM images of hydrophobic aminated silica spheres homogeneously covered with Ag nanoparticles (d) and amphiphilic Janus silica spheres with only the amine-grafted patches labeled with Ag nanoparticles (e).

diameter of 450 nm. At this size the particles are small enough to efficiently stabilize PEs while also still being large enough to easily visualize any morphology changes with TEM. The SiO_2 particles were first grafted with (3-aminopropyl)triethoxysilane (APS; Scheme 2a) to obtain base-functionalized particles (SiO_2–NH_2) with an NH_2 loading of 2.50 mmol g^{-1}. The FT-IR spectrum of the particles (see the Supporting Information, Figure S1) shows both the OH-stretch vibration of the silanol groups (3688 cm^{-1}) and the N–H stretch vibration of the amine groups (3411 cm^{-1}).

As SiO_2–NH_2 is intrinsically hydrophilic (water contact angle of 80°; SiO_2 precursor: 48.6°, Figure S4), it was necessary to partially hydrophobize the surface to favor adsorption at the oil-water interface. Reversible hydrophilization has been reported using molecular surfactants such as cetrimonium bromide (CTAB)[54] or didodecyldimethylammonium bromide (DDAB)[53,55] to tune the contact angle of the hydrophilic silica spheres, but the introduction of surfactants may have unpredictable effects on catalysis.[56] Therefore, here we used hexamethyldisilazane (HMDS)[57] instead to irreversibly hydrophobize the SiO_2–NH_2 silica spheres (Scheme 2a). The hydrophobization was confirmed in the IR spectrum by the intense C–H stretch and C–H bending vibrations of the grafted methyl groups around 2800 cm^{-1} and 1400 cm^{-1} (Figure S1b). The water contact angle for the SiO_2–NH_2–$OSi(CH_3)_3$ was found to be 135°, confirming its hydrophobicity (Figure S4).

Hydrophobized amine-functionalized SiO_2–NH_2–$OSi(CH_3)_3$ was then used as starting material for the synthesis of the acid-base Janus particles (Scheme 2b). The SiO_2–NH_2–$OSi(CH_3)_3$ particles were mixed with water and molten paraffin wax at 80 °C to form a wax-in-water PE stabilized by the SiO_2–NH_2–$OSi(CH_3)_3$ particles. Upon cooling down to room temperature, the wax solidified and colloidosomes covered with silica particles were obtained. The exposed part of the partially embedded particles was first etched with 1 wt.% HF to remove both surface functional groups (–NH_2 and –$OSi(CH_3)_3$; Figure 1b, c). As shown by TEM, the Janus silica particles are nonspherical after etching, as indicated in Figure 1b in which the original size of the sphere before (indicated by black circle) and after etching (red) is highlighted. The grey cap at the top indicated the part protected from etching inside the solidified wax; the thickness of the layer etched away was about 20 nm thick.

The etched silica was then refunctionalized by covalent grafting with various concentrations of 2-(4-chlorosulfonylphenyl)ethyltrimethoxysilane (CSPTMS). Finally, hydrolysis of chlorosulfonyl groups with HCl gave the desired sulfonic acids[58] to generate the Janus A–B particles, with a tunable SO_3H loading that ranged from 1.38 to 2.73 mmol g^{-1}.

As previously reported by Freire ad co-workers, the incorporation of phenyl sulfonic acids using this CSPTMS precursor led to a higher acid concentration and required less synthesis steps than when phenyltriethoxysilane or phenyltrimethoxysilane were used as precursor, which require sulfonation or chlorosulfonation steps in order to obtain acid functionality.[59] The FT-IR spectra before and after etching, grafting and hydrolysis, and drying the samples 400 °C under vacuum, are shown in Figure S1. The drying procedure was less effective for the acid-functionalized particles than for the SiO_2 particles, leaving a broad band from 3600 to 3000 cm^{-1} originating from water interacting with the silanol groups. The C–H stretch vibrations from the ethyl tail of the CSPTMS were observed at 3000–2700 cm^{-1} while the ring vibrations of the phenyl group were observed at ~1500 cm^{-1}.[59] Sulfonation was confirmed by the weak band corresponding to the S=O stretch vibration at 1400–1350 cm^{-1}. The water contact angle for the Janus A–B material was found to be 110° (Figure S4).

As direct visualization of grafted APS and CSPTMS is not possible with electron microscopy techniques, various other experiments were performed to show that the two parts of the Janus particle are in fact differently functionalized. For example, taking advantage of the amine groups on the surface of the silica spheres, amine functionalized silica spheres were dispersed in silver nitrate solution and *in situ* coated with silver nanoparticles (Ag np) by sodium borohydride reduction. As anticipated, the aminated silica were homogeneously covered with silver nanoparticles (Figure 1d). Conversely, coating of the etching particles lead to silver nanoparticles deposition onto the amine-functionalized patch of the Janus spheres only. No Ag np's were detected on the etched patches, confirming the Janus nature (Figure 1e).

Moreover, to show the solidified wax PE method is a general approach towards bifunctional Janus sphere synthesis, aryl-functionalized Janus spheres were prepared in a similar approach. The silica spheres were coated with a vinyl layer using 3-(trimethoxysilyl)propyl methacrylate (TPM) as silane coupling agent, on which polystyrene (PS) was grafted via seeded polymerization (Figure 2). Without etching, PS was fully grown around the vinyl-coated SiO_2, as shown in Figure 2 (left), with the dark core corresponding to the silica sphere and the grey area corresponding to PS. When the particles were partially etched, no polystyrene was detected on the etched side of the particles (Figure 2, right). The morphology of the grafted PS varies from a spherical cap to irregular cluster-like structures on the surface of the silica core, as the polymerization procedure is very sensitive to the concentrations of vinyl groups on the surface and the amount of monomers and initiators used.[60] As we were primarily interested in demonstrating the efficiency of bifunctional Janus particle synthesis, precise control over the shape of the grafted polystyrene was not necessary and therefore not further investigated. Indeed, the growth of PS again showed that the silica particles can be selectively etched and grafted using the solidified paraffin wax method.

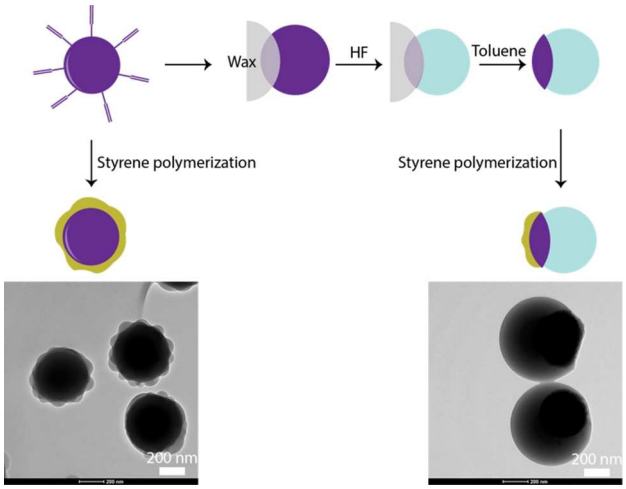

Figure 2. Schematic representation of styrene polymerization on vinyl-terminated SiO_2 particles on homogeneous functionalized particles (left) and etched Janus particles (right) with corresponding TEM images after polymerization.

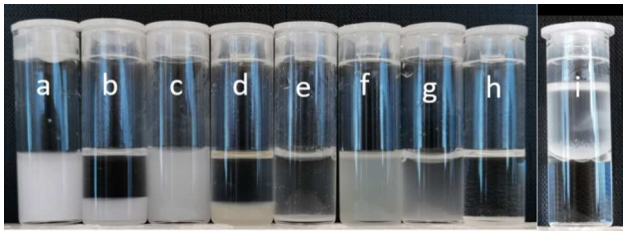

Figure 3. Unmodified SiO_2 in water (a) and toluene (b); SiO_2–NH_2 in water (c) and toluene (d); SiO_2–NH_2–$OSi(CH_3)_3$ in water (e) and toluene (f); Janus A–B in water (g) and toluene (h). Amphiphilic Janus A–B particles quickly adsorbed at the water/toluene interface (i).

To further substantiate the influence of each modification step on the properties of the material, we simply observed the stability of the dispersion in water and toluene, indeed noting the changes in behavior anticipated for the specific modification. It was found that unmodified silica (SiO_2) and aminated silica particles (SiO_2–NH_2), bearing hydrophilic surface silanols and amines, could only be dispersed in the water phase (Figure 3a–d). Particles hydrophobized with HMDS (SiO_2–NH_2–$OSi(CH_3)_3$) were found to disperse well only into the toluene phase (Figure 3e, f). The Janus silica particles did not disperse well into either water or toluene phase (Figure 3g, h) and rapidly transferred to the interface of water and toluene (Figure 3i), again corroborating that the desired Janus geometry was indeed achieved by the selective etching and coating strategy. The synthesis of the amphiphilic bifunctional Janus particles with acid functionalization on the hydrophilic and base functionalization on the hydrophobic side of the particles, to the best of our knowledge, has not been reported before.

Antagonistic tandem catalysis

With the bifunctional Janus A–B emulsifiers in hand, we set out to use them as catalysts for a tandem dehydration-Knoevenagel condensation reaction in PEs formulated with 4-propylguaiacol (PG) as organic phase and an aqueous phase saturated with sodium chloride. The alkylphenol PG was selected as the organic solvent over a more standard alkane or cyclohexane oil for its high 5-HMF extraction efficiency,[61,62] while NaCl was added to take advantage of the salting out effect to improve the partitioning of HMF into the extracting phase.[63,64] We first investigated the ability of Janus spheres to stabilize w/o PEs of PG. At 3.5 wt% silica, full PEs were obtained (Figure 4a), whereas lower emulsifier concentrations (1–3%) did not give full emulsification (Figure S2). Optical microscopy images and confocal fluorescence microscopy (CFM) images showed a

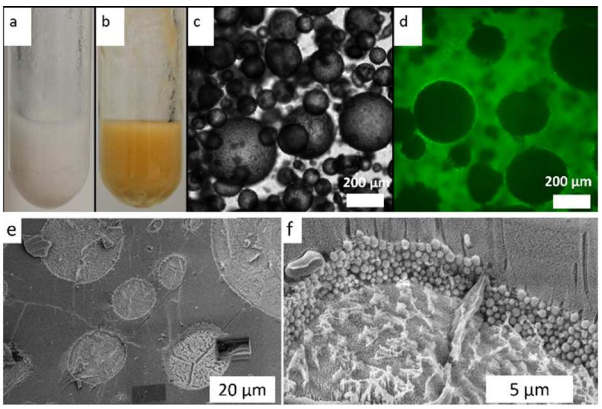

Figure 4. a, b) Physical appearance of the water/PG PE stabilized with 3.5 wt.% Janus A–B immediately after preparation (a) and after 24 h tandem catalysis (b). c) Optical microscopy image of the PE. d) Confocal fluorescence microscopy (CFM) image of the PE with the oil phase stained with Nile red. Scale bars of panels c and d = 200 µm. e, f) Low- and high-magnification cryo-SEM image of water/PG PE stabilized with Janus A–B.

broad droplet size distribution with droplet diameters varying between 50 and 300 μm (Figure 4c, d). As the organic phase was stained with Nile red, the CFM images confirmed that the PE is of the w/o type (Figure 4d). Due to the amphiphilic nature of the particles, the particles furthermore behave differently at the water/oil interface than the monofunctionalized ones. The hydrophobic amine-modified SiO_2–NH_2–$OSi(CH_3)_3$ material was also found to stabilize a PG/water PE at 3.5 wt.% (Figure S5).

As expected, the Janus A–B-stabilized Pickering emulsion was fully resistant against destabilization phenomena such as coalescence, creaming, and sedimentation, also under the more severe reaction conditions (Figure 4b). The morphology and droplet size were well retained even after a 24 h tandem reaction at 100 °C. Furthermore, cryo-SEM images were recorded to further characterize the location of the Janus particles at the oil-water interface and the solid layer structure of the PE. As can be seen from Figure 4e and f, sample preparation for cryo-SEM caused the water droplets of the PE to turn into sharp ice crystals, surrounded by a solid monolayer consisting of closely packed Janus A–B particles (Figure 4f). This dense packing of the Janus A–B particle layer is thought to contribute significantly to the observed excellent PE stability. Unfortunately, the uncontrolled fracture propagation and irregular interfacial surface topography prevented the exact configuration of Janus particles at the oil-water interface to be determined in more detail. The cross-section image in Figure S3 clearly shows that silica spheres concentrated at the interphase as a monolayer, whereas very few silica spheres are observed inside the droplets.

The compartmentalization by patch-specific functionalization should prevent acid-base quenching with these particles and we decided to perform the tandem conversion at the optimal temperature for fructose dehydration, which is 100 °C. Three different Janus A–B particles with a fixed amine concentration of 2.14 mmol, and varying acid concentration (see above) were used for catalysis (Figure 5). The Janus particles with the lowest acid concentration (1.38 mmol g^{-1}, $R_{base/acid}$ = 1.55) showed 54.3 % conversion of fructose and 5-HMF and 5-HMFDEM yields of 12.9 and 17.3 %, respectively, after 24 h. Increasing the acid concentration (2.37 mmol g^{-1}, $R_{base/acid}$ = 0.9) resulted, as expected, in higher fructose conversion, 62.6 %, but not in an increase in 5-HMF or 5-HMFDEM yield. This is indicative of an increase in humins side product formation instead. In line with this, using the Janus A–B materials with the highest acid loading (2.73 mmol g^{-1}, $R_{base/acid}$ = 0.78) led to dark coloration already after 7 h of reaction. The excessive humins formation suggests that the follow up base-catalyzed reaction was not sufficiently rapid to avoid side reactions. Indeed, even though fructose conversion was as high as 70.4 % already after 7 h reaction, the yield of 5-HMFDEM was only 11.9 %. While these first results showed that the Janus A–B can indeed be used as Pickering stabilizers and as heterogeneous catalysts for the tandem catalytic dehydration-Knoevenagel condensation reaction, they also emphasized that a fine balance needs to be struck to efficiently couple the individual steps. The second step in the tandem therefore needed to be enhanced, so a higher base/acid ratio was required.

Given the materials obtained over the different steps of the synthesis protocol, a very convenient way to tune the base/acid ratio is to use a physical mixture of the Janus A–B particles and their amine-only SiO_2–NH_2–$OSi(CH_3)_3$ precursor. Note that the latter was shown to catalyze the Knoevenagel condensation of 5-HMF and diethyl malonate (Figure S6); a combination of the amine-only material and HCl did not allow for tandem catalysis, indicating rapid quenching and highlighting the need for the use of immobilized catalysts.

While keeping the total amount of particles fixed, mixing 1 part the Janus A–B and 3 parts of the SiO_2–NH_2–$OSi(CH_3)_3$ (NH_2 loading 2.5 wt.%; total $R_{base/acid}$ = 3.53) gave a > 20 % increase of 5HMF-DEM yield (32.1 %) and a 37 % increase in selectivity (54 %; Figure 6, middle) compared to the pure Janus A–B system

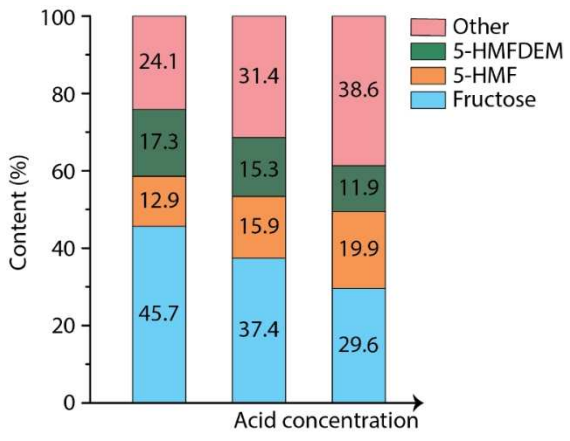

Figure 5. Product distribution of the fructose dehydration-Knoevenagel condensation tandem reaction in PEs stabilized with acid-base Janus particles with increasing acid concentration. Reaction conditions: 2 mL PG, 3.5 wt.% particles, 2 mL H_2O (30 % NaCl), 0.5 mmol fructose, 1.25 mmol diethylmalonate 100 °C; left and middle: 24 h, right: 7 h.

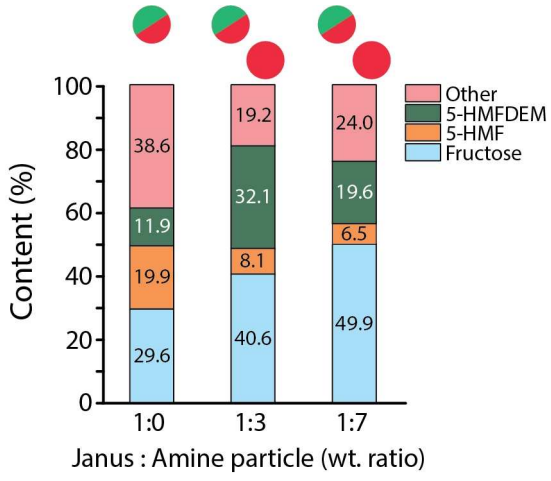

Figure 6. Product distribution of the fructose dehydration-Knoevenagel condensation tandem reaction in PEs stabilized with Janus A–B and SiO_2–NH_2–$OSi(CH_3)_3$ (red circle). Reaction conditions: 2 mL PG, 3.5 wt.% particles, 2 mL H_2O (30 % NaCl), 0.5 mmol fructose, 1.25 mmol diethylmalonate, 100 °C; left: 7 h, middle and right 24 h.

(Figure 6, left). Further increasing the amount of base catalysts by mixing 1 part of Janus A–B and 7 parts of SiO_2–NH_2–OSi $(CH_3)_3$ led to a decrease in both conversion of fructose (51.1%) and 5-HMF-DEM yield (19.6%; Figure 6, right), with the acid now likely limiting conversion in the PE system. First recycling studies showed that the material can be recovered and reused, but further optimization is required as a gradual drop in efficiency was also noted (Figure S7).

Conclusion

In summary, this study outlines a general route to fabricate bifunctional silica spheres featuring tailored functionality and asymmetric wettability through a solidified wax PE method. By using functional silica seed particles, a series of bifunctional Janus silica spheres were prepared. The versatility of the method is illustrated by the synthesis of polymer-grafted as well as nanoparticle decorated materials. Notably, compared to the reported Janus-type particles functionalized with a single-catalytic functionality,[29,37–39] the method outlined here allows bifunctional Janus silica spheres to be synthesized with tunable catalyst loading, such as the sulfonic acid and amine decorated ones used here. The inherent combination offered by Janus A–B to control spatial catalyst distribution and compartmentalization as well as to allow good emulsion stability suggests that the method presented here may be further adopted to produce various useful task-specific materials.

As first proof of concept, we demonstrated that the Janus A–B could be used as Pickering stabilizers and heterogeneous catalysts for the tandem catalytic dehydration-Knoevenagel condensation reaction of fructose. As is typical for such reactions, a fine balance needed to be struck to efficiently couple the individual steps. The specific choice for using PE as reaction medium offered a simple method to tune the acid-base catalyst ratio by stabilizing the emulsion with a physical mixture of monofunctional and Janus A–B particles. In this case, the use of such a physical mixture resulted in a considerable increase in yield and selectivity. We envision that the developed approach will serve as a versatile starting point for the synthesis of tailored multifunctional solid catalysts, which can serve as a platform for the immobilization of a variety of catalytic functionalities. The capability to orthogonally tune the properties of well-defined regions on a single colloidal particle offers the prospect of new applications in the fields of tandem catalysis, directed colloidal assembly and multiresponsive self-propelling particles.

Experimental Section

Materials. All chemicals were used as received without further purification. Hydrochloric acid (HCl, 37%, analytical grade), 4-propylguaiacol (PG, ≥99%, food grade), paraffin wax, 5-(hydroxymethyl)furfural (5-HMF, ≥99%), sodium dodecyl sulfate (SDS), styrene, potassium persulfate (KPS), ethanol, tetraethyl orthosilicate (TEOS), (3-aminopropyl)triethoxysilane (APS, ≥99%), 3-(trimethoxysilyl)propyl methacrylate (TPM, 98%), hexamethyldisilazane (HMDS), hydrofluoric acid (HF, 48%) and boric acid were purchased from Sigma-Aldrich. Anisole (99%), citric acid (99.5%), 2-(4-chlorosulfonylphenyl)ethyltrimethoxysilane (CSPTMS, 50% in dichloromethane) and ammonium hydroxide (25%) were obtained from Acros Organics. D-fructose (99%) was purchased from Alfa Aesar. Sodium chloride (NaCl) was obtained from Merck.

Synthesis of monodisperse silica spheres (SiO_2). Monodisperse surface functionalized silica spheres were synthesized using a modification of the method reported by Zhang et al.[65] In a 100 mL round bottom flask, 11.6 mL of ammonium hydroxide and 48.4 mL of ethanol were stirred at 400 rpm for 10 min. This is followed by the addition of a mixture of 1.5 mL TEOS and 6 mL of ethanol. To grow the silica particles into the desired size, 4 mL of TEOS in 20 mL of ethanol was added dropwise after 2 h of reaction. The mixture was then mechanically stirred overnight for another 24 h at room temperature. Finally, the mixture was centrifuged and washed three times with 30 mL ethanol for the complete removal of reactants.

Synthesis of amine or vinyl-decorated silica spheres (SiO_2–NH_2). Typically, 10 g of APS was added to 60 mL of toluene dispersion containing 3 g of silica spheres, and the suspension was subsequentially transferred to the oil bath to react for 24 h at 95 °C. Then the solid was collected by centrifugation and redispersion in 50 mL ethanol for three times and dried using a rotary evaporator. Similarly, the modification of silica spheres whose external surfaces covered with vinyl groups were prepared using the same method, but now using TPM as silane coupling agent.

Hydrophobization of aminated silica spheres

HMDS (2 mL) was added to 50 mL SiO_2–NH_2 ethanol dispersion containing 3 g aminated silica spheres and the suspension was stirred for 24 h. After modification, the resulting particles were washed several times with 50 mL ethanol to remove unreacted chemicals and dried in the oven at 110 °C.

Preparation of wax-water colloidosomes stabilized with silica spheres

The wax-water colloidosomes stabilized with silica spheres were prepared using a modification of a method first developed by Hong et al.[52] 0.5 g of the hydrophobized aminated silica particles (SiO_2–NH_2–$OSi(CH_3)_3$) were dispersed in 10 g of paraffin wax at 80 °C, followed by addition of 50 mL preheated water (80 °C) under magnetic stirring at 1600 rpm. After stirring for 1 h, the wax-water PE was allowed to cool down to room temperature without stirring. The resulting solid colloidosomes stabilized by hydrophobized aminated silica particles creamed up forming a white layer of small spheres during cooling procedure. The colloidosomes were washed with water to remove particles in the aqueous solution as well as weakly attached particles, then washed with 50 mL ethanol another 3 times and finally dried at room temperature.

Preparation of Janus silica by selective etching

10 g of the dried colloidosome spheres were immersed into 30 mL of 1 wt.% aqueous HF for 12 h in a plastic test tube (caution: HF solution is very hazardous and corrosive and should be handled with great care according to the MSDS guidelines), and the resulting etched Janus silica-covered colloidosomes were collected with filter paper and rinsed carefully and thoroughly with saturated boric acid aqueous solution and demi water multiple times. The colloidosomes were then dried inside a fume hood before further modification.

Synthesis of Janus silica with acidic and basic groups (Janus A–B)

The etched colloidosomes were dispersed into 30 mL ethanol solution containing 1 mL of CSPTMS and 0.5 mL ammonium hydroxide (25 wt.%) to modify the etched hemisphere. The mixture was stirred for 24 h after which the colloidosomes were washed with water three times, followed by dispersion in 30 mL 2 M HCl solution to activate the sulfonyl groups. Finally, to release these modified silica particles from the paraffin wax, the colloidosome were dispersed in toluene at 80 °C.

Synthesis of Janus SiO_2/Ag composite colloids

10 mg of the Janus colloid were firstly dispersed in ethanol (1 mL) under ultrasonication for 20 minutes (Janus A–B could not be dispersed in water directly), then 10 mL of water was added to the dispersion. After gentle shaking, a homogeneous Janus silica dispersion was obtained upon which 0.5 mL of $AgNO_3$ aqueous solution (20 mM) was added. The mixture was placed in the ultrasonic batch for another 30 min before 0.2 mL of $NaBH_4$ solution (10 mg mL^{-1}) was added dropwise. The color of the dispersion turned green/brown immediately. The product was separated by centrifugation and washed three times each with ethanol.

Synthesis of Janus SiO_2/PS composite colloids

10 mg of the Janus colloid, 4 μL of 20 wt.% SDS solution and 0.1 mL styrene were added to 2 mL water. The mixture was purged with nitrogen to remove oxygen and then emulsified with ultrasonication for 30 s. The polymerization was initiated by 200 μL KPS aqueous solution (1 wt.%) in the oil bath at 70 °C for 10 h. The product was separated by centrifugation and washed three times each with water and ethanol.

Solids characterization

Transmission electron microscopy (TEM) pictures were taken with a Philips Tecnai10 electron microscope typically operating at 100 kV. The samples were prepared by drying a drop of diluted aqueous dispersion on top of polymer-coated copper grids. Scanning electron microscopy (SEM) images were taken with a Philips SEM XL PEG 30 typically operating at 5–10 kV. The silica particles were analyzed by Fourier-Transformed Infrared (FT-IR) for which self-supported wafers of ~20 mg was mounted in an FT-IR cell connected to an oven. The wafer was dried by heating the sample to 400 °C with a heating rate of 5 °C min^{-1} under vacuum. A Perkin-Elmer System 2000 instrument was used to record the FT-IR spectra in transmission mode in the spectral range of 4000 to 1000 cm^{-1}. For each spectrum 32 scans were collected with a spectral resolution of 4 cm^{-1}. Water contact angle (CA) measurements were performed by using an FTA-1000 drop shape instrument (First Ten Angstroms Inc.). Samples were pressed to form a pellet which was then transferred to a glass slide. A 10 μL water droplet was placed on the sample pellet and the CA values were estimated by the measurement software according to the fitting method using the Young-Laplace equation.

Cryo-SEM images were taken using an Aquilos dual beam scanning electron microscope (FIB-SEM) from Thermo Scientific. Approximately 100 μL water-in-oil PE was brought into the tip of a thin plastic pipette tip and submerged into liquid nitrogen. A fresh fracture was created at the end of the pipette using pliers under liquid nitrogen and directly loaded onto the pre-cooled stage within the FIB-SEM chamber. To achieve better conductivity for imaging, Pt was sputter coated onto the fracture inside the instrument at 10 Pa with 30 mA for 10 sec to give a layer approximately 10 nm thick. Throughout the coating and imaging the temperature of the sample was kept below −170 °C. Cross sections were obtained using the Ga ion source at 30 kV in three steps: i) 15 μm × 10 μm × 5 μm (*xyz*) at 1 nA; ii) 15 μm × 2 μm × 5 μm (*xyz*) at 0.3 nA; and iii) 12 μm × 2 μm × 5 μm (*xyz*) at 0.1 nA using the Si cleaning cross section preset. For imaging, the electron beam was operated at 5 kV and 0.1 nA, with a working distance of 6.7 mm and the stage was oriented at an angle of 52° with respect to the incoming beam. Secondary electrons were captured using an Everhart-Thornley detector and backscattered electrons using a through-the-lens detector.

PE preparation

All PEs were prepared by first dispersing a known mass of particles into PG using a VCX 130 Vibra-Cell Ultrasonic Processor equipped with a 3 mm diameter tip (Sonics, 20 kHz, 10 W, 2 min). During sonication, it was necessary to cool the vessel in an ice-bath. After the addition of 2 mL aqueous phase with the appropriate NaCl concentration and after setting the required pH to the dispersion, the resulting mixture was emulsified using a UltraTurrax T25 homogenizer with a S25 N-10G dispersing tool (IKA, 15200 rpm, 2 min).

Tandem catalytic reactions

15 mL Ace pressure tubes were charged with 2 mL PG with hydrophobized aminated silica or Janus A–B. Fructose or 5-HMF dissolved in the aqueous phase were added to the pressure tubes and the PEs were prepared via emulsification for 1 min at 10 krpm using an IKA UltraTurrax with an S25N 10G dispersing tool. The PEs were left for reaction at 100 °C without stirring for the applied reaction time. After the reaction time was complete, the mixture was cooled to room temperature in air and 1 mL of citric acid solution was added (15 mg mL^{-1}) and the PE was destabilized by centrifugation using a Rotina 38-R Hettich centrifuge (11000 rpm, 4 °C, 10 min). The aqueous phase was analyzed by HPLC analysis performed on a Shimadzu HPLC system equipped with a Bio-Rad Aminex HPX-87H column, and a differential refractometer using citric acid as internal standard. The organic phase was analyzed on a Varian GC equipped with a VF-5 ms capillary column and an FID detector.

Acknowledgements

This work is part of an NWO VIDI project with project number 723.013.001, which is financed by the Dutch Research Council (NWO). Silvia Zanoni (UU) and Xinwei Ye (UU) are acknowledged for taking the FT-IR spectra. Faranaaz Rogier (UU) and Mohd Azeem Khan (UU) are acknowledged for taking the confocal microscopy images. Bonny Kuipers (UU), Kordula B. Schnabl (UU) and Cesar III Reyes (Carmalt/Parkin Group, UCL) are acknowledged for their help with the water contact angle measurements.

Conflict of Interest

The authors declare no conflict of interest.

Keywords: acid-base catalysts · biomass · emulsions · heterogeneous catalysis · Janus spheres

[1] J.-C. Wasilke, S. J. Obrey, R. T. Baker, G. C. Bazan, *Chem. Rev.* **2005**, *105*, 1001–1020.
[2] T. L. Lohr, T. J. Marks, *Nat. Chem.* **2015**, *7*, 477–482.
[3] W. Luo, W. Cao, P. C. A. Bruijnincx, L. Lin, A. Wang, T. Zhang, *Green Chem.* **2019**, *21*, 3744–3768.
[4] S. Luo, Z. Zeng, G. Zeng, Z. Liu, R. Xiao, M. Chen, L. Tang, W. Tang, C. Lai, M. Cheng, B. Shao, Q. Liang, H. Wang, D. Jiang, *ACS Appl. Mater. Interfaces* **2019**, *11*, 32579–32598.
[5] C. Han, P. Meng, E. R. Waclawik, C. Zhang, X.-H. Li, H. Yang, M. Antonietti, J. Xu, *Angew. Chem. Int. Ed.* **2018**, *57*, 14857–14861; *Angew. Chem.* **2018**, *130*, 15073–15077.
[6] L.-C. C. Lee, J. Lu, M. Weck, C. W. Jones, *ACS Catal.* **2016**, *6*, 784–787.
[7] J. Gao, X. Zhang, Y. Lu, S. Liu, J. Liu, *Chem. Eur. J.* **2015**, *21*, 7403–7407.
[8] Z. Wang, X. Yuan, Q. Cheng, T. Zhang, J. Luo, *New J. Chem.* **2018**, *42*, 11610–11615.
[9] Z. Jia, K. Wang, B. Tan, Y. Gu, *ACS Catal.* **2017**, *7*, 3693–3702.
[10] Z. Weng, T. Yu, F. Zaera, *ACS Catal.* **2018**, *8*, 2870–2879.
[11] M. B. Gawande, A. Goswami, T. Asefa, H. Guo, A. V. Biradar, D.-L. Peng, R. Zboril, R. S. Varma, *Chem. Soc. Rev.* **2015**, *44*, 7540–7590.
[12] G.-H. Wang, K. Chen, J. Engelhardt, H. Tüysüz, H.-J. Bongard, W. Schmidt, F. Schüth, *Chem. Mater.* **2018**, *30*, 2483–2487.
[13] S. Xiong, R. Tang, D. Gong, Y. Deng, C. Zhang, J. Zheng, M. Zhong, L. Su, L. Yang, C. Liao, *Appl. Mater. Res.* **2020**, *21*, 100798.
[14] J. Liu, S. Z. Qiao, J. S. Chen, X. W. Lou, X. Xing, G. Q. Lu, *Chem. Commun.* **2011**, *47*, 12578.
[15] M. Zhao, K. Deng, L. He, Y. Liu, G. Li, H. Zhao, Z. Tang, *J. Am. Chem. Soc.* **2014**, *136*, 1738–1741.
[16] P. Tundo, A. Perosa, *Chem. Soc. Rev.* **2007**, *36*, 532–550.
[17] M. Pera-Titus, L. Leclercq, J.-M. Clacens, F. De Campo, V. Nardello-Rataj, *Angew. Chem. Int. Ed.* **2015**, *54*, 2006–2021; *Angew. Chem.* **2015**, *127*, 2028–2044.
[18] F. Chang, C. M. Vis, W. Ciptonugroho, P. C. A. Bruijnincx, *Green Chem.* **2021**, *23*, 2575–2594.
[19] A. M. B. Rodriguez, B. P. Binks, *Soft Matter* **2020**, *16*, 10221–10243.
[20] C. M. Vis, L. C. J. Smulders, P. C. A. Bruijnincx, *ChemSusChem* **2019**, *12*, 2176–2180.
[21] H. Yang, L. Fu, L. Wei, J. Liang, B. P. Binks, *J. Am. Chem. Soc.* **2015**, *137*, 1362–1371.
[22] C. M. Vis, A.-E. Nieuwelink, B. M. Weckhuysen, P. C. A. Bruijnincx, *Chem. Eur. J.* **2020**, *26*, 15099–15102.
[23] F. Liang, C. Zhang, Z. Yang, *Adv. Mater.* **2014**, *26*, 6944–6949.
[24] Z. Wu, L. Li, T. Liao, X. Chen, W. Jiang, W. Luo, J. Yang, Z. Sun, *Nano Today* **2018**, *22*, 62–82.
[25] B. J. Park, D. Lee, *Soft Matter* **2012**, *8*, 7690–7698.
[26] B. J. Park, D. Lee, *ACS Nano* **2012**, *6*, 782–790.
[27] L. C. Bradley, K. J. Stebe, D. Lee, *J. Am. Chem. Soc.* **2016**, *138*, 11437–11440.
[28] F. Tu, D. Lee, *J. Am. Chem. Soc.* **2014**, *136*, 9999–10006.
[29] T. Yang, L. Wei, L. Jing, J. Liang, X. Zhang, M. Tang, M. J. Monteiro, Y. I. Chen, Y. Wang, S. Gu, D. Zhao, H. Yang, J. Liu, G. Q. M. Lu, *Angew. Chem. Int. Ed.* **2017**, *56*, 8459–8463; *Angew. Chem.* **2017**, *129*, 8579–8583.
[30] R. Koike, Y. Iwashita, Y. Kimura, *Langmuir* **2018**, *34*, 12394–12400.
[31] A. F. Mejia, A. Diaz, S. Pullela, Y. W. Chang, M. Simonetty, C. Carpenter, J. D. Batteas, M. S. Mannan, A. Clearfield, Z. Cheng, *Soft Matter* **2012**, *8*, 10245–10253.
[32] Z. Cao, G. Wang, Y. Chen, F. Liang, Z. Yang, *Macromolecules* **2015**, *48*, 7256–7261.
[33] B. P. Binks, P. D. I. Fletcher, *Langmuir* **2001**, *17*, 4708–4710.
[34] B. J. Park, T. Brugarolas, D. Lee, *Soft Matter* **2011**, *7*, 6413.
[35] T. Hessberger, L. B. Braun, R. Zentel, *Adv. Funct. Mater.* **2018**, *28*, 1800629.
[36] J. Faria, M. P. Ruiz, D. E. Resasco, *Adv. Synth. Catal.* **2010**, *352*, 2359–2364.
[37] A. Kirillova, C. Schliebe, G. Stoychev, A. Jakob, H. Lang, A. Synytska, *ACS Appl. Mater. Interfaces* **2015**, *7*, 21218–21225.
[38] J. Cho, J. Cho, H. Kim, M. Lim, H. Jo, H. Kim, S.-J. Min, H. Rhee, J. W. Kim, *Green Chem.* **2018**, *20*, 2840–2844.
[39] Y. Liu, J. Hu, X. Yu, X. Xu, Y. Gao, H. Li, F. Liang, *J. Colloid Interface Sci.* **2017**, *490*, 357–364.
[40] Y. Zhang, J. Zhang, D. Su, *J. Energy Chem.* **2015**, *24*, 548–551.
[41] B. M. Stadler, C. Wulf, T. Werner, S. Tin, J. G. de Vries, *ACS Catal.* **2019**, *9*, 8012–8067.
[42] I. Delidovich, P. J. C. Hausoul, L. Deng, R. Pfützenreuter, M. Rose, R. Palkovits, *Chem. Rev.* **2016**, *116*, 1540–1599.
[43] R.-J. van Putten, J. C. van der Waal, E. de Jong, C. B. Rasrendra, H. J. Heeres, J. G. de Vries, *Chem. Rev.* **2013**, *113*, 1499–1597.
[44] S. Tšupova, F. Rominger, M. Rudolph, A. S. K. Hashmi, *Green Chem.* **2016**, *18*, 5800–5805.
[45] Z. Xu, P. Yan, K. Liu, L. Wan, W. Xu, H. Li, X. Liu, Z. C. Zhang, *ChemSusChem* **2016**, *9*, 1255–1258.
[46] R. Lee, J. R. Vanderveen, P. Champagne, P. G. Jessop, *Green Chem.* **2016**, *18*, 5118–5121.
[47] P.-F. Koh, T.-P. Loh, *Green Chem.* **2015**, *17*, 3746–3750.
[48] Y. Yang, Z. Du, J. Ma, F. Lu, J. Zhang, J. Xu, *ChemSusChem* **2014**, *7*, 1352–1356.
[49] B. Op de Beeck, M. Dusselier, J. Geboers, J. Holsbeek, E. Morré, S. Oswald, L. Giebeler, B. F. Sels, *Energy Environ. Sci.* **2015**, *8*, 230–240.
[50] Y. Duan, J. Zhang, D. Li, D. Deng, L.-F. Ma, Y. Yang, *RSC Adv.* **2017**, *7*, 26487–26493.
[51] I. van Zandvoort, Y. Wang, C. B. Rasrendra, E. R. H. van Eck, P. C. A. Bruijnincx, H. J. Heeres, B. M. Weckhuysen, *ChemSusChem* **2013**, *6*, 1745–1758.
[52] L. Hong, S. Jiang, S. Granick, *Langmuir* **2006**, *22*, 9495–9499.
[53] S. Jiang, S. Granick, *Langmuir* **2008**, *24*, 2438–2445.
[54] A. Perro, F. Meunier, V. Schmitt, S. Ravaine, *Colloids Surf. A* **2009**, *332*, 57–62.
[55] W. Cao, R. Huang, W. Qi, R. Su, Z. He, *ACS Appl. Mater. Interfaces* **2015**, *7*, 465–473.
[56] B. Samiey, C. H. Cheng, J. Wu, *J. Chem.* **2014**, *2014*, 908476.
[57] F. Chang, S. Ouhajji, A. Townsend, K. Sanogo Lacina, B. G. P. van Ravensteijn, W. K. Kegel, *J. Colloid Interface Sci.* **2021**, *582*, 333–341.
[58] J. A. Melero, G. D. Stucky, R. van Grieken, G. Morales, *J. Mater. Chem.* **2002**, *12*, 1664–1670.
[59] M. M. Aboelhassan, A. F. Peixoto, C. Freire, *New J. Chem.* **2017**, *41*, 3595–3605.
[60] C. Zhang, B. Liu, C. Tang, J. Liu, X. Qu, J. Li, Z. Yang, *Chem. Commun.* **2010**, *46*, 4610.
[61] L. C. Blumenthal, C. M. Jens, J. Ulbrich, F. Schwering, V. Langrehr, T. Turek, U. Kunz, K. Leonhard, R. Palkovits, *ACS Sustainable Chem. Eng.* **2016**, *4*, 228–235.
[62] C. Vis, Pickering Emulsions as Compartmentalized Reaction Media for Catalysis, PhD Thesis, Utrecht University, **2020**.
[63] Y. Román-Leshkov, C. J. Barrett, Z. Y. Liu, J. A. Dumesic, *Nature* **2007**, *447*, 982–985.
[64] Y. Román-Leshkov, J. A. Dumesic, *Top. Catal.* **2009**, *52*, 297–303.
[65] J. H. Zhang, P. Zhan, Z. L. Wang, W. Y. Zhang, N. B. Ming, *J. Mater. Res.* **2003**, *18*, 649–653.

Manuscript received: June 15, 2021
Revised manuscript received: October 18, 2021
Accepted manuscript online: October 19, 2021
Version of record online: October 28, 2021